THE INFLUENCE OF MN ADDITIONS ON THE FRACTURE BEHAVIOUR OF AN AL-MG-SI ALLOY

Judith M. Dowling* and John W. Martin**

INTRODUCTION

The development of the H30 type of aluminium alloy included the addition of 0.5 wt% of Mn to the Al-Mg-Si which, due to its presence as small (< 1μm) incoherent particles of α-$Al_{12}Mn_3Si$ phase [1], reduces the tendency for intergranular embrittlement in the fully aged condition. The deformation behaviour at low plastic strains of these alloys has been studied [2], where it was concluded that the α- phase causes lateral spreading of the slip bands, giving rise to significantly smaller stress concentrations at the head of the slip bands, and whose magnitude is further reduced by the smaller grain size of the Mn-bearing material. In the latter, intergranular failure is suppressed at low strains because the stress concentrations are insufficient to produce decohesion at the grain boundary precipitates.

As well as changing the fracture path itself, the Mn-phase also influences the toughness of these alloys, and the object of the present work was to study the effect of the α- phase dispersoid on the ductile fracture process in two Al-Mg-Si alloys of different Mn content. Since commercial alloys commonly contain relatively coarse intermetallic phases containing iron, it was decided to work with high-purity (i.e. low iron) alloys, since it is considered that the coarse phases are likely to swamp effects arising from the Mn-addition [1].

MATERIALS AND METHODS

As well as the two Mn-bearing alloys, a Mn-free alloy was studied for comparison purposes, the compositions used being as follows:

Alloy	wt%Mg	Si	Fe	Mn
BD3	0.58	1.02	<0.01	0.001
BD6	0.58	0.99	<0.01	0.21
BD8	0.57	0.95	<0.01	0.50

The castings were homogenized at 530°C for 16 hours, then hot rolled at 530°C from 25mm to 10mm thickness. The billets were then cold rolled from 10mm to 3mm thickness and the final specimens were produced in the form of rods of 3.88mm diameter by swaging strips cut parallel to the rolling direction of the sheet material. Rods of gauge length 20mm were used for tensile tests.

*University of Leeds, Department of Metallurgy, Leeds, UK.
**University of Oxford, Department of Metallurgy & Science of Materials, Oxford, UK.

Test-pieces were solution-treated in air at 560°C for 30 minutes, and water quenched. After a standard age at room temperature for 5 minutes the material was aged in a molten salt bath at 185°C to peak hardness and water quenched. The ageing response of the alloys has been reported elsewhere [2].

RESULTS

(a) Tensile properties

Tensile tests were carried out on the three alloys in the fully aged condition at 20°C, 150°C and 185°C. The high temperature tests were carried out by immersing the straining rig into an oil bath previously heated to the required temperature. After immersion, there was a period of two minutes before the specimen reached temperature, after which the test was started.

The conventional stress-strain curves obtained for the three alloys are shown in Figure 1a,b,c. The fracture stress, the % elongation at the UTS, and the % reduction in area at fracture for the ductile alloys BD6 and BD8 at each testing temperature were as follows:

Alloy	Fracture stress (L_f/A_f) (MPa)	% Reduction in area at fracture	% elongation at UTS	Test temp. (°C).
BD6	425	23	14	20
	390	56	9	150
	379	62	7	185
BD8	633	55	11	20
	524	71	6	150
	515	73	4	185

Alloy BD3 was intergranularly brittle and showed little variation in ductility (approximately 1% elongation) at elevated temperatures. It is apparent that, at a given temperature, localized deformation always starts at a lower strain in BD8 than in BD6. In both alloys the onset of localized deformation is shifted to lower strains as the test temperature increases.

(b) Metallography

The grain size of BD3 was approximately 500μm, the grains being approximately equiaxed; the grains in BD6 and BD8 were smaller (100μm and 70μm respectively) and less regular, being elongated in the rolling direction. In all three alloys relatively coarse (1 - 5μm average diameter) inclusions originating from the cast structure were present, aligned in the rolling direction.

Fine needles of age-hardening precipitate, Mg_2Si, were dispersed within the grains, with coarser particles of this phase present in the grain boundaries. A precipitate-free zone (PFZ) of width ~ 0.1μm was observed adjacent to the grain boundaries in all the alloys. Intragranular dispersions of the α-$Al_{12}Mn_3Si$ phase existed in BD6 and BD8: these were rod-shaped with a diameter of 0.1μm, and had a random orientation and distribution. Particle size analyses of the α-$Al_{12}Mn_3Si$ phase were carried out on thin foils prepared form each alloy, and the resultant data were as follows:

Alloy	Particle diameter (μm)	Particle length (μm)	Volume fraction f_v	No./unit volume $N_v(m^{-3})$	Mean free path (λ) μm
BD6	0.1	0.3	0.4×10^{-2}	$1.8\ 10^{18}$	27.7
BD8	0.1	0.3	1.1×10^{-2}	$7.8\ 10^{18}$	8.9

In order to investigate the slip distribution in the alloys, thin foils were prepared from the fractured test-pieces, and these were examined using TEM. The dislocation structures were compared with those in BD3 at the same temperature. In the specimens tested at 20°C, BD3 contained well-defined slip bands with a spacing of about 3μm, while BD6 and BD8 contained a homogeneous tangle of dislocations. This type of structure has been previously reported [3]. The deformation structure of BD3 was unaltered at 185°C: the slip was still in bands, of spacing about 3μm, but the observed dislocation density was lower than after room temperature deformation. In contrast to their room temperature deformation structures, BD6 and BD8 contained well-defined slip bands (e.g. Figure 2) after high temperature deformation. The slip band spacing in each case was about 1.5μm, and the regions between the bands contained a low density of dislocations. This slip band spacing is comparable to that observed in low strains (~ 3%) at room temperature in these alloys [2].

An optical metallographic study was carried out on longitudinal sections of fractured testpieces from all three alloys. At all three temperatures, BD3 clearly fractured along its grain boundaries, and subsidiary cracks along grain boundaries, close to the plane of fracture, were observed.

The room temperature fractured test pieces of BD6 contained a number of coarse voids in the necked region, and these were often associated with narrow cracks lying at 45° to the tensile axis (Figure 3). There were also voids present in the necked region of BD8, but these were of a coarse roughly spherical variety (Figure 4) which were frequently found to be adjacent to and between the coarse residual-casting particles. Such 45° cracks as were observed in BD8 were finer and shorter than those in BD6. Their length never exceeded 10μm in BD8, whereas in BD6 the 45° cracks were between 50μm and 100μm in length.

After fracture at 150°C and 185°C a larger number of the coarse voids are seen in both BD6 and BD8; BD8 contained many voids elongated in the direction of the tensile axis (these were again seen to be in association with residual particles), whereas BD6 again showed marked evidence of prominent 45° subsidiary cracks.

(c) Fractography

At low magnifications the fracture surface of BD3 was typical of a material which has failed intergranularly. At higher magnifications the grain surfaces were seen [3] to be covered with shallow dimples which were slightly parabolic and which varied in diameter between 0.5μm and 1μm. These measurements correspond closely to the average spacing of the grain boundary precipitates in BD3.

Figures 5-7 show SEM micrographs of the room temperature fracture surfaces of BD6 and BD8. The very coarse dimples seen in Figure 6 correspond to the large voids seen optically, which are formed at the coarse residuals. On the surface of these large dimples can be seen smaller

dimples (Figure 7), about 2μm in diameter, which must arise from the presence of voids formed at some of the 0.1μm α-$Al_{12}Mn_3Si$ particles. The fracture surface of BD6 (Figure 5) also contains large dimples which correspond to voids being nucleated at coarse particles, but surface facets, 50 - 100μm across, are also present. At higher magnification these facets are not smooth, but are covered with shallow dimples about 3μm in diameter.

DISCUSSION

Stewart and Martin [4] have investigated the effect of increasing temperature on the deformation behaviour of single crystals of an Al-Si-Cu alloy which had been heat-treated to produce approximately spherical particles of Si (0.1 - 0.6μm in diameter). After deformation at room temperatures and below they found that primary dislocations were produced at the particles and also secondary dislocations in regions above and below the particles which intersected the primary slip planes. The initial work hardening rates in this temperature range were high. Deformation at temperatures above room temperature reduced the dislocation activity on the secondary slip planes, and the dislocations were confined within the primary slip planes - this process being accompanied by a sudden drop in the rate of work-hardening at about 100°C, because no dislocation debris was produced at the particles, since the particles were by-passed by a local climb process.

Since the alloys BD6 and BD8 in the present work contain similarly-sized intermetallic particles to the silicon particles in Stewart and Martin's crystals, similar changes in work-hardening rates at elevated temperatures might also be expected. Since slip homogenization by the α-$Al_{12}Mn_3Si$ particles is thought to arise from the locally high work hardening rate on the slip planes due to the accumulation of dislocation debris at the particles, elevated temperature deformation might be expected to change this response, by analogy with Stewart and Martin's results.

As seen in Figure 2, homogenization of slip is indeed absent after elevated temperature deformation. As seen in Figure 1, however, this is not accompanied by a decrease in ductility, nor by the incidence of intergranular fracture. The reason for this is clearly that the average slip band spacing in BD6 and BD8 after strain at elevated temperatures is still much less than that observed in BD3. As discussed elsewhere [2], it is concluded that the local grain boundary stresses at the head of slip bands in BD6 and BD8 will be less than those in BD3, so that intergranular failure is not nucleated in the former alloys.

The fracture mechanism in BD3 therefore, over the entire temperature range studied may be understood in terms of the above process. Under the localized stresses at the head of the coarse slip bands, void formation at grain boundary particles takes place. The ligaments between these voids will shear at a relatively low stress level, since the matrix adjacent to the grain boundary is the soft region of the precipitate-free zone and deforms more easily than the precipitation-hardened grain interiors.

With regard to the fracture processes in BD6 and BD8, it is obvious that the coarse residual intermetallics give rise to voids, presumably because such particles are large enough to contain cracks or surface defects which can initiate fracture at relatively low stresses. The growth of these voids leads to the onset of plastic instability; since there were more coarse residuals in BD8 than in BD6 this accounts for the observed

smaller strain to the UTS in BD8. The volume fraction of fine (0.1μm) intermetallics is higher in BD8 than BD6, and this has been shown [2] to lead to a higher initial rate of work hardening in the alloy. From a simple Considère consideration, therefore, one might have expected a higher strain to UTS in BD8 than BD6, and the reverse behaviour is thought to be due to the development of voids at the coarse inclusions.

An important and significant difference between BD6 and BD8 relates to the final void linkage and fracture process, and here the effect of the 0.1μm inclusions play a critical role. In BD6, where the volume fraction of these fine inclusions is lower, numerous subsidiary 45° cracks are seen to be associated with the voids (Figure 3), and the final failure process is thought to be the interlinkage of the voids by such shear cracks. In BD8, 45° cracks are sparse, the reduction in area to fracture is greater, and it is suggested that the higher volume fraction of 0.1μm particles is acting to impede plastic flow and inhibit the formation of long 45° shear cracks in the alloy.

One important property of these fine particles of α-$Al_{12}Mn_3Si$ is evidently a high work of separation of the particle/matrix interface in the system. Extensive study of thin foils taken from material close to the final fracture failed to reveal significant particle/matrix decohesion, although one or two particles of larger-than-average size were found to be cracked. Only when the final fracture propagates, therefore, is it considered that local stress levels are sufficient to cause decohesion at the fine particles and hence the fine-scale dimples on the fracture surface (Figure 7).

Van Stone and Psioda [5] have suggested that the stress necessary for void initiation at a particle is proportional to $\lambda^{-1/2}\, f^{-1/6}$, where λ is the spacing of the void initiating particles, and f their volume fraction. Substituting the values of the mean free path and volume fraction of the 0.1μm particles in BD6 and BD8 one obtains for the ratio

$$\frac{\sigma_{void}^{(BD6)}}{\sigma_{void}^{(BD8)}} = \frac{(27.7)^{-1/2}(0.4 \times 10^{-2})^{-1/6}}{(8.9)^{-1/2}(1.1 \times 10^{-2})^{-1/6}} = \frac{1}{1.5}$$

This indicates that void nucleation at these particles in BD8 requires a greater stress than in BD6 and it is interesting to note that the ratio of fracture stresses for BD8:BD6 at room temperature is 1.5, at 150°C is 1.4 and 185°C is also 1.4. This suggests that the difficulty of void nucleation at the 0.1μm particles may be responsible for higher ductility and higher fracture stresses in BD8.

CONCLUSIONS

The difference in behaviour between BD6 and BD8 is therefore due to the difference in volume fraction of the fine dispersoids, which have the effect of inhibiting shear of the matrix. In BD6 the low volume fraction and thus large mean free path between these 0.1μm particles is such that ductile fracture can easily propagate by 45° shear between voids from cracked coarse particles. In BD8 the stress for propagating shear cracks is raised by the presence of a higher number of fine dispersoids on these planes. Further strain hardening therefore occurs until decohesion is achieved at these particles, and either 45° or 'normal' void linkage will occur. DB8 can thus support higher stresses before fracture due to the

0.1μm particles inhibiting shear fracture, so higher fracture strains and presumably higher toughness is achieved.

ACKNOWLEDGEMENTS

The authors are indebted to Messrs Alcan International Limited for material help. JMD acknowledges financial support from the Science Research Council.

REFERENCES

1. DUNWOODY, B.J., MOORE, D.M. and THOMAS, A.T., J. Inst. Metals, 101, 1973, 172.
2. DOWLING, J.M. and MARTIN, J.W., Acta Metallurgica, in press.
3. DOWLING, J.M. and MARTIN, J.W., Proc. 3rd Conf. on Strength of Metals and Alloys, Cambridge 1973, 170.
4. STEWART, A.T. and MARTIN, J.W., Acta Metallurgica, 23, 1975, 1.
5. VAN STONE, R.H. and PSIODA, J.A., Met. Trans., 6A, 1975, 669.

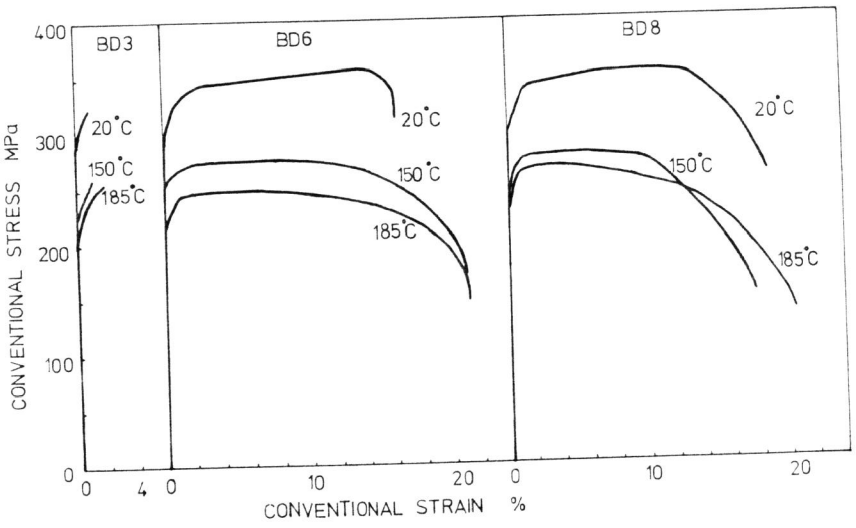

Figure 1 Conventional stress-strain curves for the three alloys at the stated temperatures

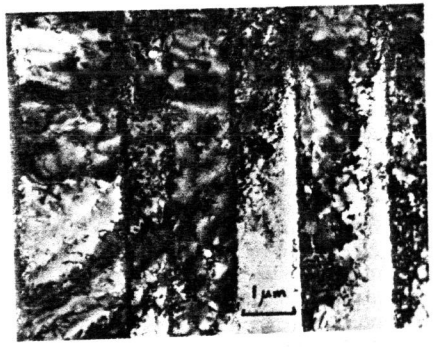

Figure 2 Transmission electron micrograph of a section from alloy BD6 after tensile fracture at 185°C

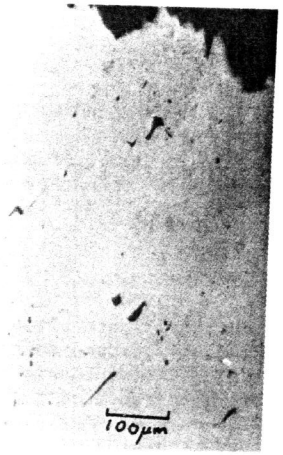

Figure 3 Longitudinal section of alloy BD6 after tensile fracture at 20°C (Optical micrograph unetched)

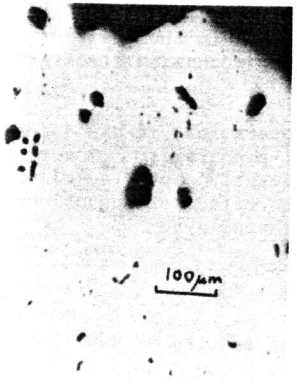

Figure 4 Longitudinal section of alloy BD8 after tensile fracture at 20°C (Optical micrograph, unetched)

Figure 5 SEM of the fracture surface (20°C) of BD6

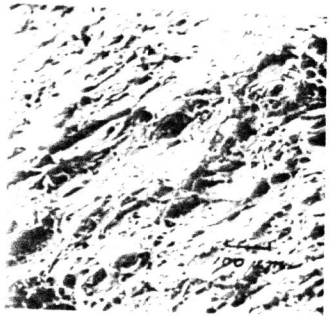

Figure 6 SEM of the fracture surface (20°C) of BD8

Figure 7 As Figure 6, higher magnification